Structure formation in mimetic gravity

Bita Farsi[1,*] and Ahmad Sheykhi[1,2,†]

[1]*Department of Physics, College of Sciences, Shiraz University, Shiraz 71454, Iran*
[2]*Biruni Observatory, College of Sciences, Shiraz University, Shiraz 71454, Iran*

(Received 8 February 2022; revised 24 June 2022; accepted 17 July 2022; published 28 July 2022)

We disclose the effects of an extra longitudinal degree of freedom on the evolution of perturbations in the framework of mimetic gravity. We consider a flat Friedmann-Robertson-Walker background and explore the linear perturbations by adopting the spherically symmetric collapse formalism. By suitably choosing the potential of the mimetic field, we are able to solve the perturbed field equations in the linear regime and derive the matter density contrast δ_m in terms of the redshift parameter z. We observe that δ_m starts growing at the early stages and, as the Universe expands, it grows faster compared to the standard cosmology. This may due to the extra degree of freedom of the gravitational field which affects the growth of perturbations. We observe that in the presence of a mimetic potential, the growth rate function is smaller than the ΛCDM model in small redshifts. We then consider the effects of this potential on the density abundance, the deceleration parameter and jerk parameter. We find out that mimetic potential can play the role of dark energy (DE) and affects the dynamics of matter perturbations and cosmological parameters. We also investigate the mass function and the number count for the collapsed objects in the mimetic scenario. We find that the mass function of models with potential is smaller than the model without potential. With the decreasing the role of DE, the mass function starts to grow in smaller redshifts; i.e., halo abundance is formed later. It is found that the more massive structures are less abundant and form at later times, as it should be in the hierarchical model of structure formation.

DOI: 10.1103/PhysRevD.106.024053

I. INTRODUCTION

Einstein's theory of general relativity (GR) is one of the foundations of modern physics along with the quantum field theory [1]. Until now, GR has successfully passed various excremental and observational tests such as bending of light, gravitational time dilation, gravitational lensing, precession of the Mercury orbit, etc. [2]. Another successful prediction of GR is the existence of the gravitational waves which was detected directly from merging of black holes in the Laser Interferometer Gravitational-Wave Observatory (LIGO) [3]. This detection, a century after the theory was established by Einstein in 1915, is a great achievement in science and opens a new window, gravitational-wave observatory, to look at the Universe. Despite the huge success of GR, it still suffers to explain some cosmological observations such as the flat galaxies rotation curves [dark matter (DM) puzzle], the initial and the black hole singularities and the accelerated expansion of the Universe [dark energy (DE) puzzle]. Therefore, either alternative theories of gravity or new components of matter/energy have been proposed to explain the observed phenomenons.

Modified gravity theories have achieved great development and performance in the explanation of some unsolved problems of GR. One of the modifications to GR is the mimetic theory of gravity which was suggested as a new explanation for the DM puzzle [4]. In this scenario, a mimetic scalar field Φ is introduced which is not dynamical by itself, nevertheless it makes the longitudinal degree of freedom of the gravitational field dynamical. This dynamical longitudinal degree of freedom of the gravitational field can play the role of mimetic pressureless DM [4]. A modified version of mimetic gravity can address the cosmological singularities [5] as well as the singularity in the center of a black hole [6]. Besides, it has been confirmed that the original setting of the mimetic theory predicts that the gravitational wave (GW) propagates at the speed of light, ensuring agreement with the results of the event GW170817 and its optical counterpart [7–9]. It has also been shown that this theory can explain the flat rotation curves of spiral galaxies without needing to particles DM [10,11]. The mimetic theory of gravity has raised a lot of enthusiasm in the past few years both from the cosmological viewpoint [12–31] as well as black holes physics [32–51]. The investigations on the mimetic theory of gravity were also generalized to $f(R)$ gravity [52–65] as well as Gauss-Bonnet gravity [66–70]. In particular, a unified description of early inflation and late-time

*Bita.Farsi@shirazu.ac.ir
†asheykhi@shirazu.ac.ir

acceleration in the context of mimetic $f(R)$ gravity was established in [71]. It has been confirmed that in the background of mimetic $f(R)$ gravity, the inflationary era can be realized [71].

Observations confirm that almost 26% of the energy budget of the Universe corresponds to the DM sector, while around 69% constitutes the DE [72]. There are enough evidences that support the existence of DM and DE in the Universe [73]. DE has became relevant only more recently and is presumed to be a smooth component with a negative pressure. DE has an antigravity feature and pushes the Universe to accelerate and therefore is responsible for the acceleration of the cosmic expansion (for a recent review on DE and DM see [74]). DM plays two important roles in the Universe evolution. First it provides enough gravity for the rotation of the spiral galaxies as well as cluster of galaxies. Second, it plays a crucial role in the growth of perturbation and structure formation in the early stage of the Universe. The latter is due to the fact that DM has no electromagnetism interaction (no photon radiation) while it enjoys the gravitational interaction. As a result, DM begins to collapse into a complex network of DM halos, while ordinary matter continues its collapse due to the photon radiation and finally settles down into the well potential of the DM. Without DM, the epoch of galaxy formation would occur substantially later in the Universe than is observed.

Understanding the origin and physics of the growth of perturbations in galaxies and clusters of galaxies has been one of the main challenges of modern cosmology. This is of great importance, since these perturbations eventually lead the large scale structure of the Universe. It is a general belief that the large scale structure of the Universe such as galaxies and clusters of galaxies arise from gravitational instability that amplifies very small initial density fluctuations during the Universe evolution. Such fluctuations then grow slowly over time until they get robust enough to be detached from the background expansion. Finally, they collapse into gravitationally bound systems such as galaxies and clusters of galaxies. In other words, the primordial collapsed regions serve as the initial cosmic seeds for which the large scale structures are developed [75,76].

An appropriate approach to investigate the growth of perturbations and structure formation is the so-called top-hat spherical collapse (SC) model. The results of the observational data [77] show that most of the structures are formed from nonlinear evolution of perturbations in the dark age period ($10 < z < 100$) [78]. The dark age is the period between the time when the cosmic microwave background was emitted and the time when the evolution of structure in the Universe led to the gravitational collapse of objects, in which the first galaxies were formed. The simplest analytical approach to study nonlinear structure formation is the SC model [79]. In this model, one considers a uniform and symmetrical spherical perturbation in an expanding background. The symmetry of this model allows us to treat a spherical perturbation in a Friedmann-Robertson-Walker (FRW) universe. In other words, we can describe the growth of perturbations in a spherical region using the same Friedmann equations for the underlying theory of gravity [80]. According to the SC model, at early times, primordial spherical overdense regions expand along the Hubble flow. Since the relative overdensity of the overdense region with respect to the background is small, the linear theory is enough to study their evolution. At a certain point, gravity starts dominating and overcomes the expansion rate. Eventually, the sphere reaches a maximum radius and completely detaches from the background expansion. The following phase is represented by the collapse of the sphere under its own self-gravity. The exact process of collapse due to gravitational instability depends strongly on the dynamics of the background Hubble flow [81]. The effects of DE on the structure formation has been investigated in various scenarios [82]. In the context of mimetic gravity, the cosmological perturbations have been investigated in [83]. Our work differs from [83] in that instead of using the Newtonian gauge, we use SC formalism to examine the evolution of perturbations.

The outline of this paper is as follows. In Sec. II, we provide a review on mimetic gravity and derive the corresponding Friedmann equations in the context of mimetic cosmology. In Sec. III, using the spherically collapse approach, we explore the growth of matter perturbation in the background of flat mimetic cosmology. In Sec. IV, we study the mass function and number count of the collapsed objects in the mimetic scenario. The last section is devoted to the conclusion and discussion.

II. MIMETIC COSMOLOGY

According to the mimetic theory of gravity, the physical metric $g_{\mu\nu}$ is related to the auxiliary metric $\tilde{g}_{\mu\nu}$ and scalar field Φ through a conformal transformation [4]

$$g_{\mu\nu} = \tilde{g}_{\mu\nu}\tilde{g}^{\alpha\beta}\partial_\alpha\Phi\partial_\beta\Phi, \tag{1}$$

where the physical metric $g_{\mu\nu}$ is invariant under the conformal transformations of the auxiliary metric $\tilde{g}_{\mu\nu}$, namely, under $\tilde{g}_{\mu\nu} \to \Omega^2\tilde{g}_{\mu\nu}$, we have $g_{\mu\nu} \to g_{\mu\nu}$.

The action of mimetic gravity in the presence of a mimetic potential is given by [14]

$$S = \int d^4x\sqrt{-g}\left[\frac{R}{2\kappa^2} + \frac{\lambda}{2}(\partial^\mu\Phi\partial_\mu\Phi - 1) - V(\Phi) + \mathcal{L}_{\rm m}\right], \tag{2}$$

where R is the Ricci scalar, $\mathcal{L}_{\rm m}$ is the Lagrangian of matter, g is the determinant of the physical metric, and λ is a Lagrange multiplier. Here $V(\Phi)$ is an arbitrary function of the scalar field Φ, and the factor $1/2$ in front of the Lagrange multiplier λ is introduced for later convenience.

Such a model has been shown to provide an economical way of reproducing a number of simple and well-motivated cosmological scenarios, relevant for both early- and late-time cosmology, without the need for neither an explicit DM nor dark fluid [12]. Throughout this work, we take $\kappa^2 = 8\pi G = 1$, for simplicity. By varying the above action with respect to the physical metric $g_{\mu\nu}$, one can derive the field equations as [14]

$$G_{\mu\nu} + \lambda\partial_\mu\Phi\partial_\nu\Phi + g_{\mu\nu}V(\Phi) = T_{\mu\nu}, \tag{3}$$

where $G_{\mu\nu}$ is the Einstein tensor and $T_{\mu\nu}$ is the energy momentum tensor of the usual matter. Variation of the action (2) with respect to Lagrange multiplier λ yields

$$g^{\mu\nu}\partial_\mu\Phi\partial_\nu\Phi = 1. \tag{4}$$

This constraint, which is consistent with conformal transformation (1), implies that the scalar field is not dynamical by itself, however, it encodes a new longitudinal degree of freedom to the gravitational field [4]. By varying action (2) with respect to the mimetic field Φ, we find [14]

$$\nabla^\mu(\lambda\partial_\mu\Phi) + \frac{dV}{d\Phi} = 0. \tag{5}$$

This equation can also be derived by taking the covariant derivative of Eq. (3) and using the fact that $\nabla^\mu G_{\mu\nu} = 0$, together with the continuity equation $\nabla^\mu T_{\mu\nu} = 0$. We also assume the background is homogeneous, isotropic and spatially flat with line elements,

$$ds^2 = dt^2 - a^2(t)(dx^2 + dy^2 + dz^2), \tag{6}$$

where $a(t)$ is the scale factor of the Universe and we have taken the spacetime signature as $(+,-,-,-)$. For homogenous cosmology, the mimetic scalar field is only a function of time, i.e., $\Phi = \Phi(t)$. Inserting into condition (4) immediately yields

$$\dot{\Phi}^2 = 1. \tag{7}$$

Integrating (assuming $\dot{\Phi} > 0$), we get $\Phi = t$, where we have also set the integration constant equal to zero. We further assume the energy content of the Universe is in the form of perfect fluid with energy-momentum tensor $T^\mu_\nu = \mathrm{diag}(\rho, -p, -p, -p)$, where ρ and p are, respectively, the energy density and pressure of the fluid. Conservation of the energy-momentum tensor, $\nabla^\mu T_{\mu\nu} = 0$, in the background of a FRW universe leads to

$$\dot{\rho} + 3H(\rho + p) = 0. \tag{8}$$

So the energy density of the pressureless matter can be written as $\rho_m = \rho_{m,0}a^{-3}$. The cosmological field equations can be derived by substituting the metric (6) and the energy momentum tensor in the field Eqs. (3) and (5). We find [14]

$$3H^2 = \rho - \lambda - V, \tag{9}$$

$$3H^2 + 2\dot{H} = -(p + V), \tag{10}$$

$$\dot{\lambda} + 3H\lambda + \frac{dV}{d\Phi} = 0, \tag{11}$$

where $H \equiv \dot{a}/a$ is the Hubble parameter. Let us note that we can distinguish three sectors for the energy components. First is the usual matter with energy density ρ and pressure p. The second is the mimetic field which plays the role of DM and contributes through λ in the field equations. Third is the mimetic potential, V, which plays the role of DE. The first Friedmann equation (9), using the definition of density parameters, can be rewritten

$$\Omega_m + \Omega_\lambda + \Omega_V = 1, \tag{12}$$

$$\Omega_m \equiv \frac{\rho_m}{3H^2}, \tag{13}$$

$$\Omega_{dm} \equiv \Omega_\lambda \equiv \frac{-\lambda}{3H^2}, \tag{14}$$

$$\Omega_{de} \equiv \Omega_V \equiv \frac{-V}{3H^2}. \tag{15}$$

Using the fact that $\Phi = t$, Eq. (11) can be written as

$$\frac{d\lambda}{d\ln a} + 3\lambda + \frac{dV}{d\ln a} = 0. \tag{16}$$

Thus, if we make the following ansatz for the potential,

$$V(a) = -\frac{\beta}{1+\beta}\lambda(a), \tag{17}$$

then we can solve analytically Eq. (16) to arrive at

$$\lambda(a) = \lambda_0 a^{-3(1+\beta)}, \tag{18}$$

where β is a dimensionless constant and λ_0 is the present value of λ, and we have chosen $a_0 = a(t = t_0) = 1$. Hence the explicit form of the mimetic potential is given by

$$V(a) = -\frac{\beta\lambda_0}{\beta+1}a^{-3(1+\beta)}. \tag{19}$$

In the absence of the mimetic potential ($\beta = 0 = V$), from Eq. (18) one can see that $\lambda = \lambda_0 a^{-3}$, namely the field mimics DM [4].

As we shall see the mimetic potential indeed plays the role of DE and can lead to the acceleration of the cosmic expansion. Besides, in our model, we assumed the mimetic

potential (which plays the role of DE) is a function of λ (which plays the role of DM). This implies an interaction between DE and DM. The Hubble expansion rate can be obtained via Eq. (9) as

$$H^2 = \frac{\rho_{m,0}(1+\beta) - \lambda_0 a^{-3\beta}}{3(1+\beta)a^3}. \tag{20}$$

So we can define the normalized Hubble parameter as

$$E(z) = \frac{H(z)}{H_0} = \sqrt{\frac{\rho_{m,0}(1+\beta) - \lambda_0(1+z)^{3\beta}}{3H_0^2(1+\beta)(1+z)^{-3}}} = \sqrt{\frac{[(1+\beta) + \frac{\Omega_{\lambda,0}}{\Omega_{m,0}}(1+z)^{3\beta}](1+z)^3}{(1+\beta) + \frac{\Omega_{\lambda,0}}{\Omega_{m,0}}}}. \tag{21}$$

The evolution of the normalized Hubble parameter versus z for different values of β is plotted in Fig. 1.

In Fig. 2, we have plotted the evolution of the density abundance Ω_m, defined as

$$\Omega_m(z) = \frac{\rho_m}{3H^2} = \frac{(1+\beta)\rho_{m,0}}{(1+\beta)\rho_{m,0} - \lambda_0(1+z)^{3\beta}} = \frac{(1+\beta)\Omega_m^0}{(1+\beta)\Omega_m^0 + \Omega_\lambda^0(1+z)^{3\beta}}. \tag{22}$$

As we can see from Fig. 2, the matter density abundance with different β parameters has the same behavior at first, i.e., all graphs are reduced by decreasing z. In addition for smaller values of β parameter, the density abundance drops faster.

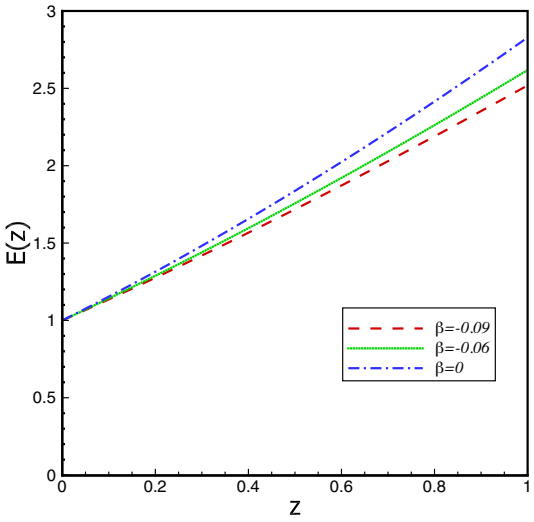

FIG. 1. The behavior of the normalized Hubble rate for different values of β.

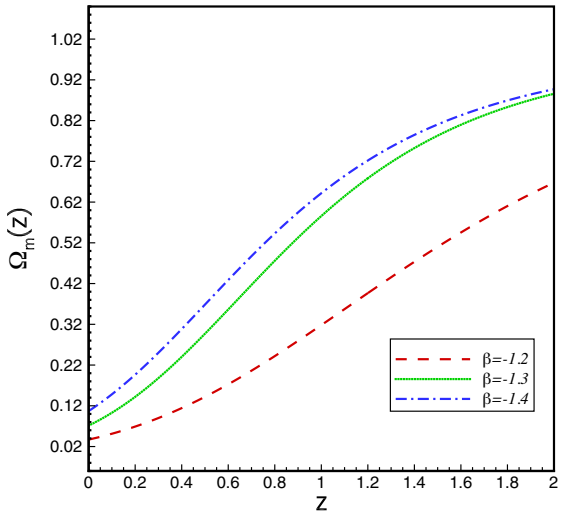

FIG. 2. The evolution of the matter density abundance as a function of redshift z for different values of β.

We can also write the explicit expression for Ω_λ as

$$\Omega_\lambda(z) = \frac{-\lambda}{3H^2} = \frac{-\lambda_0(1+\beta)(1+z)^{3\beta}}{(1+\beta)\rho_{m,0} - \lambda_0(1+z)^{3\beta}} = \frac{(1+\beta)\Omega_\lambda^0(1+z)^{3\beta}}{(1+\beta)\Omega_m^0 + \Omega_\lambda^0(1+z)^{3\beta}}. \tag{23}$$

In a similar way, the evolution of the density abundance Ω_V is given by

$$\Omega_V(z) = \frac{-V}{3H^2} = \frac{\beta\lambda_0(1+z)^{3\beta}}{(1+\beta)\rho_{m,0} - \lambda_0(1+z)^{3\beta}} = -\frac{\beta\Omega_\lambda^0(1+z)^{3\beta}}{(1+\beta)\Omega_m^0 + \Omega_\lambda^0(1+z)^{3\beta}}. \tag{24}$$

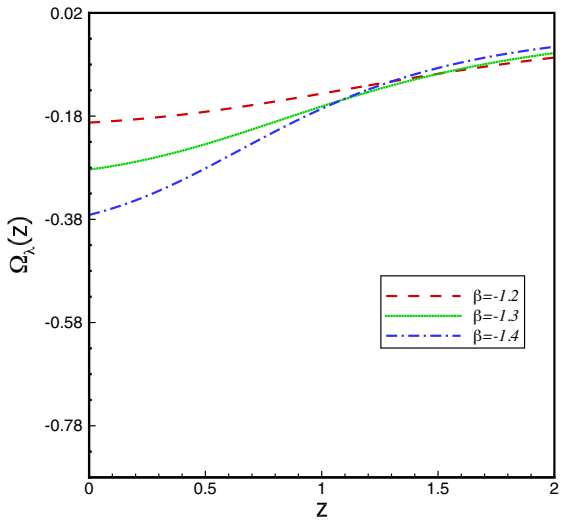

FIG. 3. The evolution of the DM density abundance in terms of the redshift z for different values of β.

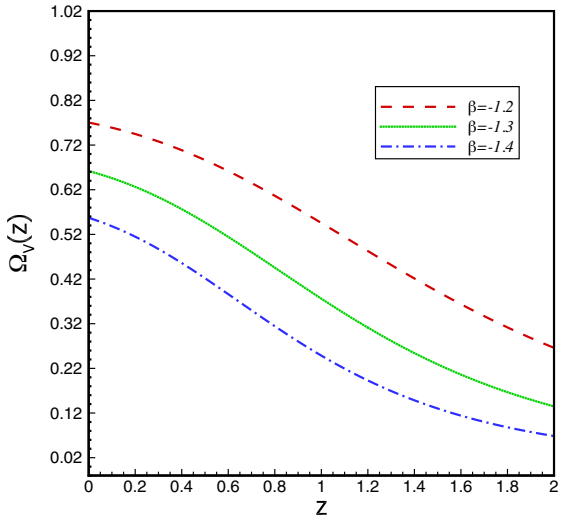

FIG. 4. The evolution of the DE density abundance in terms of the redshift z for different values of β.

As we can see from Figs. 2–4, in the framework of mimetic gravity, the different potential suggests different values for Ω_m^0, Ω_λ^0 and Ω_V^0. Comparing to standard values of the density parameters, i.e., $\Omega_m^0 = 0.05$, $\Omega_\lambda^0 = 0.26$ and $\Omega_V^0 = 0.69$, we find that the best value for the β parameter is $\beta \simeq -1.3$, which corresponds to the ΛCDM model.

The deceleration parameter in terms of the redshift can be written as

$$q = -1 - \frac{\dot{H}}{H^2} = -1 + \frac{(1+z)}{H(z)}\frac{dH(z)}{dz}, \tag{25}$$

Using Eq. (20) the deceleration parameter is given by

$$q(z) = \frac{1}{2}\left[\frac{(\beta+1)\rho_{m,0} - (3\beta+1)\lambda_0(1+z)^{3\beta}}{(\beta+1)\rho_{m,0} - \lambda_0(1+z)^{3\beta}}\right]. \tag{26}$$

Let us note that for either $\beta = 0$ or $\lambda_0 = 0$, we have $q = 1/2$, which is the result of standard cosmology in the presence of dust. We have plotted the behavior of the deceleration parameter $q(z)$ for different β parameters in Fig. 5. We observe that the Universe experiences a transition from decelerating phase ($z > z_{\rm tr}$) to accelerating phase ($z < z_{\rm tr}$), where $z_{\rm tr}$ is the redshift at the transition point. Also we can see that with decreasing β, the phase transition between deceleration and acceleration takes place at lower redshifts. Note that $q(z)$ has a phase transition, for different values of β, forming deceleration ($q > 0$) to acceleration ($q < 0$) phase, around $z \approx 0.6$ which is compatible with observational data.

Another quantity which is helpful in understanding the phase transitions of the Universe expansion is called the jerk parameter. This is a dimensionless quantity obtained by taking the third derivative of the scale factor with respect to the cosmic time, providing a comparison between

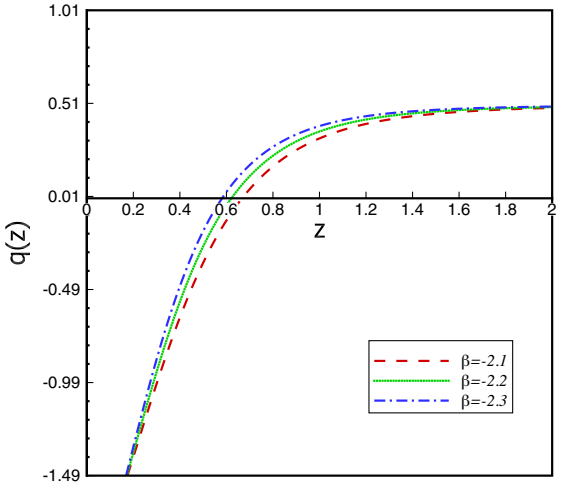

FIG. 5. The behavior of the deceleration parameter as a function of redshift for different β.

different DE models and the ΛCDM ($j = 1$) model. The jerk parameter is defined as [84–86]

$$j = \frac{1}{aH^3}\frac{d^3a}{dt^3} = q(2q+1) + (1+z)\frac{dq}{dz}. \tag{27}$$

As we know the Hubble parameter, the deceleration parameter and the jerk parameter are purely kinematical, since they are independent of any gravity theory, and all of them are only related to scale factor a or redshift z. For the ΛCDM model, the value of j is always unity. A non-ΛCDM model occurs if there is any deviation from the value of $j = 1$. This is similar as deviation from the equation of state parameter $\omega = -1$, for other DE models. Using Eq. (25) in Eq. (27), we can find the jerk parameter in our model. From Fig. 6 we observe the jerk parameter at

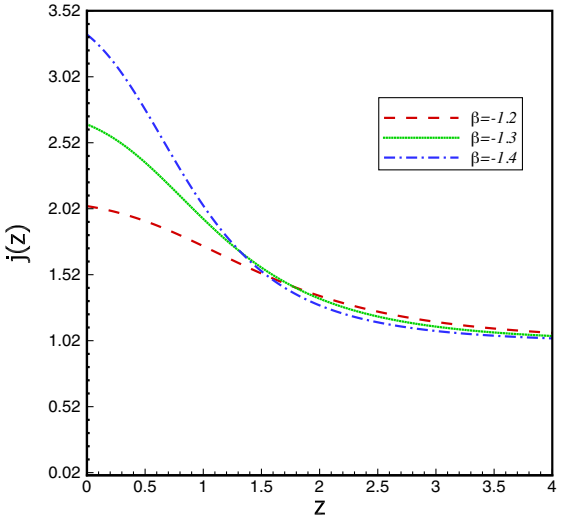

FIG. 6. The evolution of jerk parameter with respect to redshift for different values of β parameter.

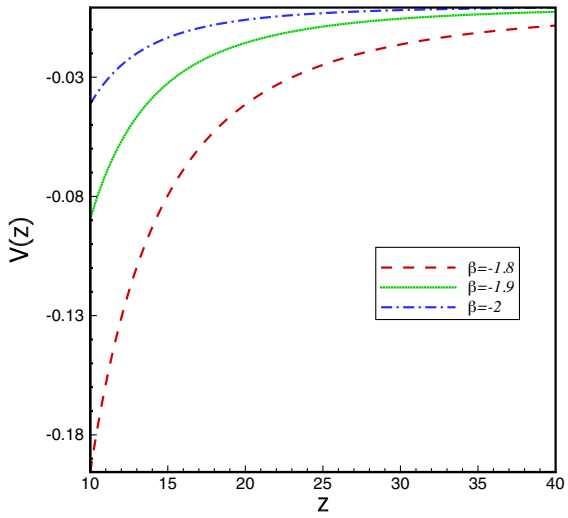

FIG. 7. The behavior of the mimetic potential in terms of the redshift parameter for different β.

early time ($z > 1$) tends to a ΛCDM model ($j = 1$). Finally, we can plot the mimetic potential given in Eq. (19) as a function of redshift parameter. From Fig. 7, we observe that as the Universe expands, the potential increases from the past to the present.

III. GROWTH OF PERTURBATION IN MIMETIC COSMOLOGY

We consider a universe filled with pressureless matter, $p = p_m = 0$. In this case Eq. (8) reads

$$\dot{\rho}_m + 3H\rho_m = 0, \tag{28}$$

which has a solution of the form $\rho_m = \rho_{m,0}a^{-3}$, where $\rho_{m,0}$ is the energy density at the present time. In order to study the growth of perturbations, we consider a spherically symmetric perturbed cloud of radius a_p, and with a homogeneous energy density ρ_m^c. The SC model describes a spherical region with a top-hat profile and uniform density so that at any time t, we can write $\rho_m^c(t) = \rho_m(t) + \delta\rho_m$ [87]. If $\delta\rho_m > 0$ this spherical region will eventually collapse under its own gravitational force and if $\delta\rho_m < 0$ it will expand faster than the average Hubble expansion rate, thus generating a void. In other words, $\delta\rho_m$ is positive in the overdense region and it is negative in underdense regions. In fact, when the Universe is in the matter dominated era, denser regions expand slower than the entire Universe. Therefore if their density is enough large, they eventually collapse and create gravitational constraint systems like clusters [88]. Similar to Eq. (28), the conservation equation for a spherical perturbed region can be written as

$$\dot{\rho}_m^c + 3h\rho_m^c = 0, \tag{29}$$

where $h = \dot{a}_p/a_p$ is the local expansion rate of the spherical perturbed region of radius a_p (subscript p refers to the perturbed). In order to study the evolution of perturbations, we define a useful and dimensionless quantity called density contrast as [88]

$$\delta_m = \frac{\rho_m^c}{\rho_m} - 1 = \frac{\delta\rho_m}{\rho_m}, \tag{30}$$

where ρ_m^c is the energy density of the spherical perturbed cloud and ρ_m is the background density. Taking the derivative of Eq. (30) with respect to the cosmic time and using Eqs. (28) and (29) we obtain

$$\dot{\delta}_m = 3(1 + \delta_m)(H - h), \tag{31}$$

$$\ddot{\delta}_m = 3(\dot{H} - \dot{h})(1 + \delta_m) + \frac{\dot{\delta}_m^2}{1 + \delta_m}, \tag{32}$$

where the dot denotes the derivative with respect to time. Combining Eqs. (9), (10), (19) and (18), we arrive at

$$\frac{\ddot{a}}{a} = -\frac{1}{6}\left(\rho_m + \left(\frac{-1 + 3\beta}{1 + \beta}\right)\lambda_0 a^{-3(1+\beta)}\right). \tag{33}$$

According to the SC model, a homogeneous sphere of uniform density with radius a_p can itself be modeled using the same equations that govern the evolution of the Universe, with scale factor a [75]. Therefore, we can write for the spherical perturbed cloud with radius a_p, an equation similar to Eq. (33), namely

$$\frac{\ddot{a}_p}{a_p} = -\frac{1}{6}\left(\rho_m^c + \left(\frac{-1 + 3\beta}{1 + \beta}\right)\lambda_0^c a_p^{-3(1+\beta)}\right). \tag{34}$$

In general, one may expect λ_0 and β differ inside and outside of the spherical region. However, for simplicity here we propose they are similar, namely $\lambda_0^c = \lambda_0$ and $\beta^c = \beta$. Consider two spheres with equal amounts of material, one of background material with radius a, and one of radius a_p with a homogeneous change in overdensity, so we have $\rho_m^c a_p^3 = \rho_m a^3$ [88]. Combining with Eq. (30), we get

$$a_p = a(1 + \delta_m)^{-1/3}. \tag{35}$$

Therefore, Eq. (34) can be rewritten as

$$\begin{aligned}\frac{\ddot{a}_p}{a_p} &= -\frac{1}{6}\left\{\rho_m^c + \left(\frac{-1 + 3\beta}{1 + \beta}\right)\lambda_0 a^{-3(1+\beta)}(1 + \delta_m)^{1+\beta}\right\} \\ &= -\frac{1}{6}\left\{\rho_m^c + \left(\frac{-1 + 3\beta}{1 + \beta}\right)\lambda_0 a^{-3(1+\beta)}[1 + (1 + \beta)\delta_m]\right\},\end{aligned} \tag{36}$$

where we have expanded the last term and only kept the linear term of δ_m. This is due to the fact that we work in the linear regime where $\delta_m < 1$. Combining Eqs. (33) and (36) yields

$$\dot{H}-\dot{h}=\frac{1}{6}\delta_m[\rho_m+(-1+3\beta)\lambda_0 a^{-3(1+\beta)}]-H^2+h^2. \tag{37}$$

Substituting Eq. (37) into Eq. (32) and using Eq. (31), we can find the second order differential equation for the density contrast δ_m as

$$\ddot{\delta}_m-\frac{1}{2}[\rho_m+(-1+3\beta)\lambda_0 a^{-3(1+\beta)}]\delta_m(1+\delta_m) -\frac{4}{3}\frac{\dot{\delta}_m^2}{1+\delta_m}+2H\dot{\delta}_m=0, \tag{38}$$

where the matter energy density is given by $\rho_m=\rho_{m,0}a^{-3}$. In order to study the evolution of the density contrast δ_m in terms of the redshift parameter, $1+z=1/a$, we first replace the time derivatives with the derivatives with respect to the scale factor a. It is a matter of calculations to show that

$$\dot{\delta}_m=\delta_m' aH, \qquad \ddot{\delta}_m=\delta_m'' a^2H^2-\frac{1}{2}a(H^2-V)\delta_m', \tag{39}$$

where the prime stands for the derivative with respect to a. Therefore Eq. (38) with using Eq. (9) can be written as

$$\delta_m''+\frac{3}{2a}\delta_m'+\frac{1}{2aH^2}(-3H^2+\rho_m-\lambda_0 a^{-3(1+\beta)})\delta_m' -\frac{1}{2a^2H^2}\delta_m(1+\delta_m)(\rho_m+(-1+3\beta)\lambda_0 a^{-3(1+\beta)}) -\frac{4}{3}\frac{{\delta_m'}^2}{(1+\delta_m)}=0. \tag{40}$$

Since we are working in the linear regime, thus we neglect $O(\delta_m^2)$ and $O({\delta_m'}^2)$. Combining Eqs. (20) and (40), we arrive at

$$\delta_m''+\frac{3}{2a}\delta_m'-\frac{3}{2a}\beta\left[\frac{\lambda_0 a^{-3\beta}}{(\beta+1)\rho_{m,0}-\lambda_0 a^{-3\beta}}\right]\delta_m' -\frac{3}{2a^2}(\beta+1)\left[\frac{\rho_{m,0}+(-1+3\beta)\lambda_0 a^{-3\beta}}{(\beta+1)\rho_{m,0}-\lambda_0 a^{-3\beta}}\right]\delta_m=0. \tag{41}$$

It should be noted that either in the absence of the mimetic field ($\lambda_0=0$), or in the absence of the mimetic potential ($\beta=0$), Eq. (41) reduces to

$$\delta_m''+\frac{3}{2a}\delta_m'-\frac{3\delta_m}{2a^2}=0, \tag{42}$$

which is the result obtained in standard cosmology [79]. This implies that the presence of the mimetic potential plays an important role in studying the evolution of perturbation in mimetic cosmology. In other words, in the absence of the mimetic potential, the perturbed equation for the density contrast, δ_m, in the linear regime, coincides with the ones in standard cosmology. Also in order to express δ_m as a function of z, we can change the variable from the scale factor to the redshift parameter z. In this way, Eq. (41) transforms to

$$(1+z)^2\frac{d^2\delta_m}{dz^2}+\frac{1}{2}(1+z)\frac{d\delta_m}{dz} +\frac{3}{2}(1+z)^{(3\beta+1)}\left\{\frac{\lambda_0\beta}{(1+\beta)\rho_{m,0}-\lambda_0(1+z)^{3\beta}}\right\}\frac{d\delta_m}{dz} -\frac{3}{2}(1+\beta)\left\{\frac{\rho_{m,0}+(-1+3\beta)\lambda_0(1+z)^{3\beta}}{(1+\beta)\rho_{m,0}-\lambda_0(1+z)^{3\beta}}\right\}\delta_m=0. \tag{43}$$

In this work, we assume $\Omega_m^0=0.05$, $\Omega_\lambda^0=0.26$, and $\Omega_V^0=0.69$. Thus from Eqs. (13) and (14) we have $\lambda_0/\rho_{m,0}=\Omega_\lambda^0/\Omega_m^0=+5.2$, ($\lambda_0>0$). Therefore, Eq. (43) admits the following analytical solution:

$$\delta_m(z)=\left\{C_1(1+z)^{\alpha_+}{}_2F_1\left(\eta_+,\eta_-,s_+,\frac{1923(1+\beta)}{10000(1+z)^{3\beta}}\right) +C_2(1+z)^{\alpha_-}\times{}_2F_1\left(\eta_+,\eta_-,s_-,\frac{1923(1+\beta)}{10000(1+z)^{3\beta}}\right)\right\}M, \tag{44}$$

where C_1 and C_2 are integration constants and

$$\begin{aligned}
M&=[-19230000+(3697929\beta+3697929)(1+z)^{-3\beta}]^{1/4}\\
&\quad\times[-10000+(1923+1923\beta)(1+z)^{-3\beta}]^{5/4},\\
\alpha_\pm&=\frac{1}{4}\pm\frac{1}{28}\sqrt{7}\sqrt{-175+294\beta+441\beta^2}+\frac{3}{4}\beta,\\
\eta_\pm&=-\frac{1}{84\beta}\left\{-105\beta\mp35+\sqrt{7}\sqrt{-175+294\beta+441\beta^2}\right\},\\
s_\pm&=\mp\frac{1}{42\beta}\left\{\mp42\beta+\sqrt{7}\sqrt{-175+294\beta+441\beta^2}\right\}.
\end{aligned} \tag{45}$$

To obtain the integration constants, we note that for large values of the redshift parameter, the parameter β goes to zero where the GR limit is recovered. We therefore consider the adiabatic initial conditions for matter perturbations as [79]

$$\frac{d\delta_m(z)}{dz}(|_{z=zi})=-\frac{\delta_m(z_i)}{1+z_i}, \tag{46}$$

where $\delta_m(z_i)$ is the initial value for the density contrast at $z=z_i$. In Fig. 8, we have plotted the matter density contrast

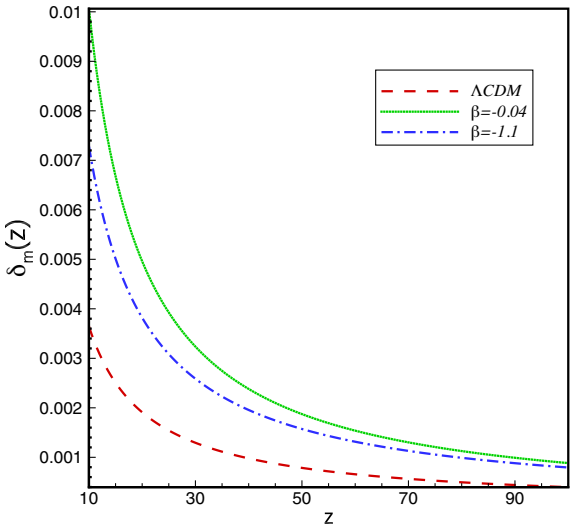

FIG. 8. The evolution of the matter density contrast for different values of β during the evolution of the Universe. We have chosen $\delta_m(z_i) = 0.0001$ and $z_i = 400$.

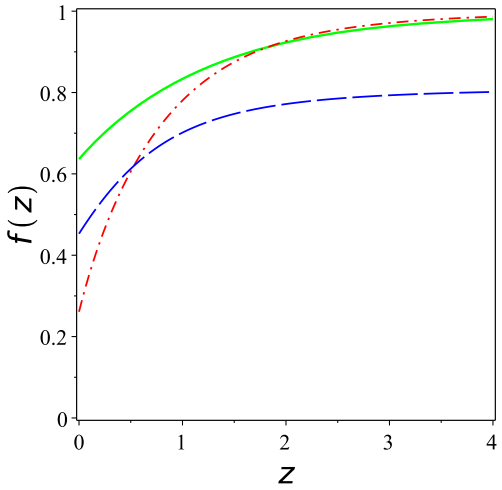

FIG. 9. The evolution of the growth function for different values of β parameter, where the solid line is for $\beta = -1.1$, the dash-dotted line is for $\beta = -1.2$, and the long dashed line is for ΛCDM.

as a function of redshift for different values of β parameter and for redshifts $10 < z < 100$. We observe that in the framework of mimetic gravity, the growth of matter perturbations is larger than the ΛCDM model. Indeed, the density contrast of matter starts growing from its initial value and, as the Universe expands, the matter density contrast grows up faster and deviates from the ΛCDM profile. We find out that the β parameter affects the growth of matter perturbations, in particular in the lower redshifts. In fact, the growth of perturbations increases with increasing β, which reveals the influences of the mimetic field. The physical reason behind this behavior comes from the fact that the mimetic field encodes an extra longitudinal degree of freedom to the gravitational field, which can support the growth of matter perturbations. We remind that the Universe goes through several phase transitions during its formative stages. Cosmic reionization is the last of them, where ultraviolet and x-ray radiation escape from the first generations of galaxies heating and ionizing their surroundings and subsequently the entire intergalactic medium [89]. This occurred between 150 million and one billion years after the big bang ($6 < z < 20$) [89]. The results suggest that the Universe was approaching the end of reionization around $z = 6$. It suggests that the Universe must still have been almost entirely neutral at $z > 10$. This is the physical reason that we take the perturbations for $10 < z < 100$ in Fig. 8 [89].

We can investigate the growth rate of matter perturbations which is given by the growth function as [75]

$$f(a) = \frac{d\ln D}{d\ln a}, \qquad D(a) = \frac{\delta_m(a)}{\delta_m(a=1)}. \tag{47}$$

Let us note that in the absence of the mimetic field ($\lambda_0 = 0$), or in the absence of the mimetic potential ($\beta = 0$), the growth function is a constant of unity. In Fig. 9 we have plotted the growth function in terms of the redshift parameter. We observe the amplitude of perturbations in high redshifts corresponds to the unity, but it starts to decrease at low redshifts similar to the ΛCDM model. Therefore, the role of potential (DE), like Λ, is to reduce the growth function from unity. Besides, the current value of $f(z)$ crucially depends on the β parameter and decreases with decreasing β.

We can also measure the growth rate matter perturbations from the redshift-space distortion of the clustering pattern of galaxies. This distortion is caused by the peculiar velocity of inward collapse motion of the large-scale structure, which is directly related to the growth rate of the matter density contrast δ_m [90]. Recent galaxy redshift surveys have provided bounds on the growth rate $f(z)$ or $f(z)\sigma_8(z)$ in terms of the redshift where $f(z)$ is from Eq. (47)) and σ_8 is the rms amplitude of δ_m at the comoving scale $8h^{-1}$ Mpc [91,92] and can be written as [93]

$$\sigma_8(z) = \frac{\delta(z)}{\delta(z=0)}\sigma_8(z=0), \tag{48}$$

where we have assumed $\sigma_8(z=0) = 0.983$ [92], and we have shown the redshift evolution of $f(z)\sigma_8(z)$ for different values of β parameter in Fig. 10. We see that the growth rate of models with potential (nonzero β) is smaller than the model without potential. Although the behavior of models with potential is similar for large redshifts, in small redshifts ($z < 1$) the model with a larger β parameter predicts a larger value of the cosmological growth rate. From Fig. 10 we observe that in small redshifts, the growth rate function with potential is smaller than the ΛCDM model. Also one can see that the evolution of the function $f\sigma_8$ for $\beta = -1.2$,

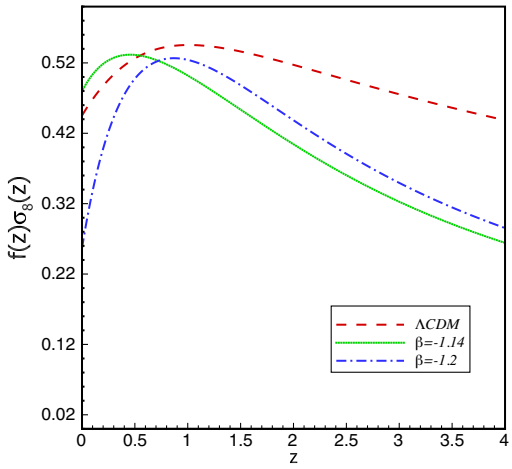

FIG. 10. The behavior of $f(z)\sigma_8(z)$ for different values of β parameter.

is very similar to the ΛCDM theory. The difference can be traced back to the linear regime of the solutions. The present value of $f\sigma_8$ for $\beta = -1.14$ is greater than of the ΛCDM value. Also we see for a larger value of β parameter $f\sigma_8$ reaches the maximum value at smaller redshifts. In other words, with increasing the role of potential (DE) the large structures have been formed later in this mimetic gravity.

IV. MASS FUNCTION AND CLUSTER NUMBER COUNTS

Besides the evolution of matter density contrast, in the present work the number count of the collapsed objects in the mimetic scenario is also emphasized. The gravitational collapse of the matter overdensity is the basic process of large scale structure formation in the Universe. The objects, formed by the collapse, are called the DM halos. Due to gravitational attraction the baryonic matter follows the distribution DM. Hence the galaxy clusters are embedded in the DM halos. The observed distribution of galaxy clusters provides the information about the distribution of DM halos in the Universe. In this section, using the SC model, we study the DM halo mass function and the number distribution in the context of mimetic cosmology.

Now we want to use the Press-Schechter approach in order to estimate the number counts of DM halos for different bins of redshifts and halo masses [94]. The Press-Schechter formalism assumes the fraction of mass in the Universe contained in gravitationally bound systems with masses greater than M is given by the fraction of space where the linearly evolved density contrast exceeds a threshold δ_c, and that the density contrast is normally distributed with zero mean and variance $\sigma^2(M)$—the root-mean-square value of the density contrast δ at scales containing mass M. Therefore, it is assumed that for a massive sphere to undergo gravitational collapse at a redshift z its linear overdensity should exceed a threshold $\delta_c(z)$. Notice that only linear quantities are used in this formalism. The key quantity in the SC is the critical overdensity $\delta_c(z_c)$ at a given collapse redshift z_c. It is defined as the value of the linear density contrast at the redshift where the nonlinear density contrast diverges. In other words it is defined as the final value (i.e., at redshift z_c) of the linear evolution of a given spherical top-hat initial perturbation that actually collapses at z_c according to the full nonlinear equations.

These assumptions lead to the well-known analytical formula for the comoving number density of collapsed halos of mass in the range M and $M + dM$ at a given redshift z [95]:

$$\frac{dn}{dM} = -\sqrt{\frac{2}{\pi}}\frac{\rho_{m,0}}{M}\frac{\delta_c(z)}{\sigma(M,z)}\frac{d\ln\sigma(M,z)}{dM}\exp\left[-\frac{\delta_c^2(z)}{2\sigma^2(M,z)}\right], \tag{49}$$

where $\rho_{m,0}$ is the present matter mean density of the Universe and $\delta_c(z)$ is the linearly extrapolated density threshold above which structures collapse, i.e., $\delta_c(z) = \delta(z_c)$. In an Einstein-de Sitter universe, an overdensity region collapses with a linear contrast $\delta_c = 1.686$ [96]. In order to obtain δ_c in terms of the redshift parameter z, we consider linear equation (41) for the spherical region where $\delta_m = \delta_c$. This equation with using the differential-radius method [97] has the solution in the form $\delta_c(a) \propto a_c^{(A+3)/4}$, in far redshifts. In other words with $1+z \propto t^{-2/3}$, we can see the time dependence $\delta_c \propto t^m$, where $m = (\sqrt{1+24\Omega_m}-1)/6$ [98]. Therefore, its solution can be written as

$$\delta_c(z) = \frac{\delta_i}{2}\left(1+\frac{1}{A}\right)\left(\frac{1+zi}{1+z}\right)^{(A-1)/4}, \tag{50}$$

where $A = \sqrt{25-72\beta}$ depends on the model parameter β. Let us note that for an initial perturbation $\delta_i = 10^{-7}$ and $1+z_i = 10^8$, and the overdensity region collapses at redshift $z_c = 2.558$, Eq. (50) gets $\delta_c = 1.686$, which corresponds to the EdS value. The quantity

$$\sigma(M,z) = D(z)\sigma_M \tag{51}$$

is the linear theory "rms" density fluctuation in spheres of comoving radius R containing the mass M, where $D(z) \equiv \delta_m(z)/\delta_m(z=0)$ is the linear growth function obtained from Eq. (47)). The smoothing scale R is often specified by the mass within the volume defined by the window function at the present time, see e.g., [75]. In our analysis the variance of the smoothed overdensity containing a mass M is given by [99]

$$\sigma_M = \sigma_8\left(\frac{M}{M_8}\right)^{-\gamma(M)/3}, \tag{52}$$

where $M_8 = 6 \times 10^{14}\Omega_M^{(0)} h^{-1}\ M_\odot$ is the mass inside a sphere of radius $R_8 = 8h^{-1}$ Mpc, and σ_8 is the variance of the overdensity field smoothed on a scale of size R_8 [99]. The index $\gamma(M)$ is a function of the mass scale and the shape parameter, Γ, of the matter power spectrum [99]

$$\gamma = (0.3\Gamma + 0.2)\left[2.92 + \frac{1}{3}\log\left(\frac{M}{M_8}\right)\right]. \quad (53)$$

In our study we use $\Gamma = 0.167$ [100].

Denoting $\tilde{\gamma}(M) = d\ln\sigma(M,z)/dM$,

$$\tilde{\gamma}(M) = (0.3\Gamma + 0.2)\left[2.92 + \frac{2}{3}\log\left(\frac{M}{M_8}\right)\right], \quad (54)$$

we can rewrite Eq. (49) as

$$\frac{dn}{dM} = -\sqrt{\frac{2}{\pi}}\frac{\rho_{m,0}}{M}\frac{\delta_c(z)}{\sigma(M,z)}\tilde{\gamma}(M)\exp\left[-\frac{\delta_c^2(z)}{2\sigma^2(M,z)}\right]. \quad (55)$$

For a fixed σ_8 (power spectrum normalization) the predicted number density of DM halos given by the above formula is uniquely affected by the DE models, with different β parameter, through the ratio $\delta_c/D(z)$. In Fig. 11, we have shown the redshift evolution of the mass function $[dn/dM(1/\mathrm{Mpc}^3)]$ of objects with mass $10^{13}h^{-1}\ M_\odot$ for different β parameter. From this figure, we can investigate the modifications caused by a DE component on the number of DM halos. We observe that the mass function of models with potential (nonzero β) starts to grow around $z \sim 2$. Besides, the mass function for $\beta = -1.01, -1.4$ is smaller than the ΛCDM model, while for $\beta = -1.4$ its present value corresponds to the ΛCDM model. Also the smaller value of β parameter gives larger halo abundances. In other words from Fig. 11, we find out that by reducing the role of DE, then the comoving number density becomes more. We can see that with decreasing the role of DE (for smaller β parameter), the mass function starts to grow in smaller redshifts; i.e., halo abundance is formed later. Also we find this same qualitative behavior within the mass range, 10^{13}–$10^{16}h^{-1}\ M_\odot$, for dark energy models with different β parameter.

The effect of dark energy on the number of DM halos is studied by computing two quantities. The first is all sky number of halos per unit of redshift, in a given mass bin [98]

$$\mathcal{N}^{bin} \equiv \frac{dN}{dz} = \int_{4\pi} d\Omega \int_{M_{\mathrm{inf}}}^{M_{\mathrm{sup}}} \frac{dn}{dM}\frac{dV}{dz d\Omega} dM, \quad (56)$$

where the comoving volume element is given by

$$\frac{dV(z)}{dz d\Omega} = \frac{r^2(z)}{H(z)}, \quad (57)$$

where $r(z) = \int_0^z H^{-1}(x)dx$ is the comoving distance. We have plotted the redshift evolution of the comoving volume element $[dV/dzd\Omega(\mathrm{Mpc}^3)]$ with different β parameter in Fig. 12. As we see the comoving volume element is larger for smaller values of β parameter. Note that the comoving volume element does not depend on the growth factor of the perturbation $D(z)$, but only on the cosmological background. The number counts in mass bins, $\mathcal{N}^{bin} = dN/dz$, obtained from Eq. (56), is shown in Fig. 13. In this figure we show it for the $\beta = 0$ model and for different mass bins $[M_{\mathrm{inf}}, M_{\mathrm{sup}}]$ as $[10^{12}, 10^{13}]h^{-1}\ M_\odot$, $[10^{13}, 10^{14}]h^{-1}\ M_\odot$,

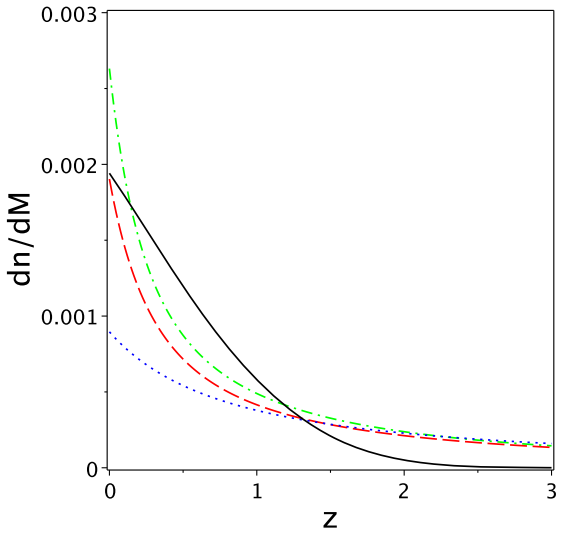

FIG. 11. The evolution of mass function for objects with mass $M = 10^{13}(h^{-1}\ M_\odot)$ with different β parameter, where the dash-dotted line is for $\beta = -1.6$, the dashed line is for $\beta = -1.4$, the dotted line is for $\beta = -1.01$ and the solid line is for ΛCDM.

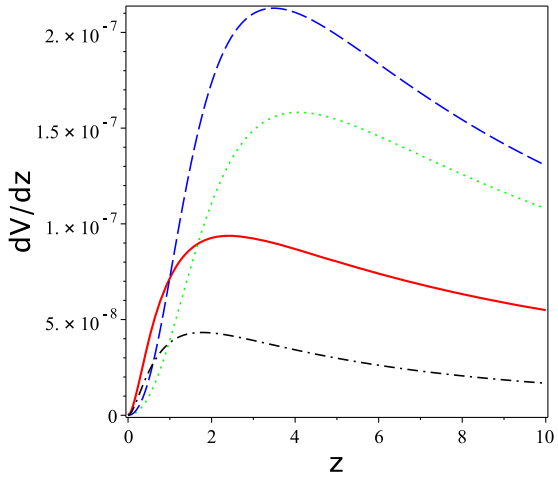

FIG. 12. The behavior of the comoving volume element with different β parameter, where the dashed line is for $\beta = -1.4$, the dotted line is for $\beta = -1.2$, the solid line is for $\beta = -0.09$, and the dash-dotted line shows it for $\beta = 0$.

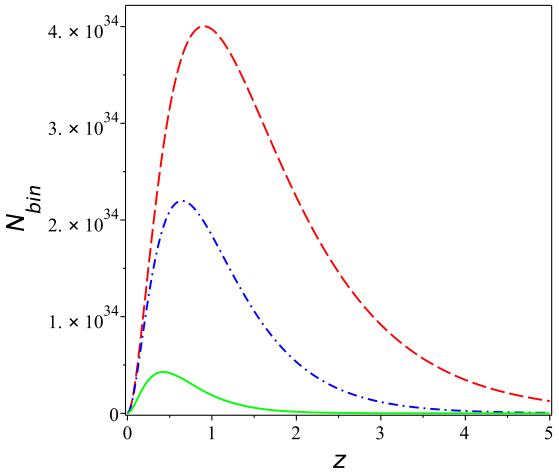

FIG. 13. The evolution of number counts with redshift from the $\beta = 0$ model for objects with mass within the range, the dashed line for $10^{12} < M/(h^{-1}M\odot) < 10^{13}$, the dash-dotted line for $10^{13} < M/(h^{-1}M\odot) < 10^{14}$, and the solid line for $10^{14} < M/(h^{-1}M\odot) < 10^{15}$.

$[10^{14}, 10^{15}]h^{-1}\ M_\odot$. As we see the more massive structures are less abundant and form at later times, as it should be in the hierarchical model of structure formation. Also the second quantity is the all sky integrated number counts above a given mass threshold, $M_{\rm inf}$ and up, to redshift [98]

$$\mathcal{N}(z, M > M_{\rm inf}) = \int_{4\pi} d\Omega \int_{M_{\rm inf}}^{\infty} \int_0^z \frac{dn}{dM}\frac{dV}{dz' d\Omega} dM dz'. \quad (58)$$

V. CONCLUSION AND DISCUSSION

The discovery that the expansion of the Universe is accelerating has led to large observational programs being carried out to understand its origin. New facilities are being designed and built aiming to measure the expansion history and the growth of structure in the Universe with increasing precision out to greater redshifts. Since the dark sectors change the expansion history of the Universe and the evolution of matter density perturbations, these new facilities will not only test the current period of accelerated expansion but also explain the nature of the dark sectors.

In this paper, we have investigated the evolution of the matter perturbations in the context of mimetic gravity for different values of the model parameters. We have employed the SC formalism in order to examine the perturbations and worked in the linear regime. We proposed the mimetic potential (which plays the role of DE) is proportional to the mimetic DM density, i.e., $V \propto \lambda$. With this ansatz, we found out $\lambda \sim a^{-3(1+\beta)}$, implying an interaction between DE and DM in this model. The density contrast has similar behavior for different values of β parameter; that is, it starts from its initial value and then it grows up at low redshifts. Besides, the density contrast grows faster for larger values of β parameter. Furthermore, as the value of the β parameter decreases, then the growth of matter perturbations is decreasing, too. In other words we see that the growth rate of models with potential (nonzero β) is smaller than the model without potential. Also we studied the modifications caused by a dark energy component on the number of DM halos as the smaller value of β parameter gives larger halo abundances. Also we see that for smaller β parameter and therefore with decreasing the role of DE, the mass function starts to grow in smaller redshifts; i.e., halo abundance is formed later. Also we see the comoving volume element is larger for smaller values of β parameter. In addition we found the number counts in mass bins for the more massive structures are less abundant and form at later times, as it should be in the hierarchical model of structure formation. We also studied the evolution of the density parameters. We observed that the evolution of the matter density abundance and the DM density abundance for different values of β decrease by decreasing the redshift. We found out that the density abundance of matter, consist of baryonic and DM, drops slower for larger values of β. From the evolution of the deceleration parameter, we see that the Universe experiences a phase transition from decelerating phase to accelerating phase around redshift $z_{\rm tr} \approx 0.6$ which is compatible with observational data.

It is interesting to constrain the model presented here by using observational data, such as observations of type Ia supernova and baryon acoustic oscillations. We leave this issue for future investigations.

ACKNOWLEDGMENTS

We are grateful to the anonymous referees for very helpful and constructive comments which helped us improve our paper significantly. We also thank H. Moradpour and M. Asghari for useful discussions and valuable comments.

[1] S. M. Carroll, *Spacetime and Geometry: An Introduction to General Relativity* (Addison-Wesley Press, Reading, MA, 2004).

[2] C. M. Will, The confrontation between general relativity and experiment, Living Rev. Relativity **9**, 03 (2006).

[3] B. P. Abbott *et al.* (LIGO Scientific, Virgo Collaborations), The Observation of Gravitational Waves from a Binary Black Hole Merger, Phys. Rev. Lett. **116**, 061102 (2016).
[4] A. H. Chamseddine and V. Mukhanov, Mimetic dark matter, J. High Energy Phys. 11 (2013) 135.
[5] A. H. Chamseddine and V. Mukhanov, Resolving cosmological singularities, J. Cosmol. Astropart. Phys. 03 (2017) 009.
[6] A. H. Chamseddine and V. Mukhanov, Nonsingular black hole, Eur. Phys. J. C **77**, 183 (2017).
[7] A. Casalino, M. Rinaldi, L. Sebastiani, and S. Vagnozzi, Mimicking dark matter and dark energy in a mimetic model compatible with GW170817, Phys. Dark Universe **22**, 108 (2018).
[8] A. Casalino, M. Rinaldi, L. Sebastiani, and S. Vagnozzi, Alive and well: Mimetic gravity and a higher-order extension in light of GW170817, Classical Quantum Gravity **36**, 017001 (2019).
[9] K. Sherafati, S. Heydari, and K. Karami, Higher order mimetic gravity after GW170817, arXiv:2109.11810.
[10] S. Vagnozzi, Recovering a MOND-like acceleration law in mimetic gravity, Classical Quantum Gravity **34**, 185006 (2017).
[11] A. Sheykhi and S. Grunau, Topological black holes in mimetic gravity, Int. J. Mod. Phys. A **36**, 2150186 (2021).
[12] A. H. Chamseddine, V. Mukhanov, and A. Vikman, Cosmology with mimetic matter, J. Cosmol. Astropart. Phys. 06 (2014) 017.
[13] E. H. Baffou, M. J. S. Houndjo, M. Hamani-Daouda, and F. G. Alvarenga, Late time cosmological approach in mimetic f(R,T) gravity, Eur. Phys. J. C **77**, 708 (2017).
[14] J. Dutta, W. Khyllep, E. N. Saridakis, N. Tamanini, and S. Vagnozzi, Cosmological dynamics of mimetic gravity, J. Cosmol. Astropart. Phys. 02 (2018) 041.
[15] A. Sheykhi, Thermodynamics of apparent horizon in mimetic cosmology, Int. J. Mod. Phys. D **28**, 1950057 (2019).
[16] M. H. Abbassi, A. Jozani, and H. R. Sepangi, Anisotropic mimetic cosmology, Phys. Rev. D **97**, 123510 (2018).
[17] J. Matsumoto, Unified description of dark energy and dark matter in mimetic matter model, arXiv:1610.07847.
[18] L. Sebastiani, S. Vagnozzi, and R. Myrzakulov, Mimetic gravity: A review of recent developments and applications to cosmology and astrophysics, Adv. High Energy Phys. **2017**, 3156915 (2016).
[19] N. Sadeghnezhad and K. Nozari, Braneworld mimetic cosmology, Phys. Lett. B **769**, 134 (2017).
[20] M. A. Gorji, S. Mukohyama, and H. Firouzjahi, Cosmology in mimetic $SU(2)$ gauge theory, J. Cosmol. Astropart. Phys. 05 (2019) 019.
[21] M. A. Gorji, S. Mukohyama, H. Firouzjahi, and S. A. Hosseini, Gauge field mimetic cosmology, J. Cosmol. Astropart. Phys. 08 (2018) 047.
[22] M. B. Lopez, C.-Y. Chen, and P. Chen, Primordial cosmology in mimetic Born-Infeld gravity, J. Cosmol. Astropart. Phys. 11 (2017) 053.
[23] M. A. Gorji, S. A. Hosseini, and H. Firouzjahi, Higher derivative mimetic gravity, J. Cosmol. Astropart. Phys. 01 (2018) 020.
[24] H. Firouzjahi, M. A. Gorji, S. A. Hosseini Mansoori, A. Karami, and T. Rostami, Two-field disformal transformation and mimetic cosmology, J. Cosmol. Astropart. Phys. 11 (2018) 046.
[25] A. H. Chamseddine, V. Mukhanov, and T. B. Russ, Asymptotically free mimetic gravity, Eur. Phys. J. C **79**, 558 (2019).
[26] T. B. Russ, On stability of asymptotically free mimetic Horava gravity, arXiv:2103.12442.
[27] M. de Cesare, S. S. Seahra, and E. Wilson-Ewing, The singularity in mimetic Kantowski-Sachs cosmology, J. Cosmol. Astropart. Phys. 07 (2020) 018.
[28] V. H. Cardenas, M. Cruz, S. Lepe, and P. Salgado, Reconstructing mimetic cosmology, Phys. Dark Universe **31**, 100775 (2021).
[29] S. A. Hosseini Mansoori, A. Talebian, and H. Firouzjahi, Mimetic inflation, J. High Energy Phys. 01 (2021) 183.
[30] F. Arroja, T. Okumura, N. Bartolo, P. Karmakar, and S. Matarrese, Large-scale structure in mimetic Horndeski gravity, J. Cosmol. Astropart. Phys. 05 (2018) 050.
[31] A. H. Mansoori, A. Talebian, Z. Molaee, and H. Firouzjahi, Large-scale structure in mimetic Horndeski gravity multi-field mimetic gravity, Phys. Rev. D **105**, 023529 (2022).
[32] N. Deruelle and J. Rua, Disformal transformations, veiled general relativity and mimetic gravity, J. Cosmol. Astropart. Phys. 09 (2014) 002.
[33] R. Myrzakulov and L. Sebastiani, Spherically symmetric static vacuum solutions in mimetic gravity, Gen. Relativ. Gravit. **47**, 89 (2015).
[34] R. Myrzakulov, L. Sebastiani, S. Vagnozzi, and S. Zerbini, Static spherically symmetric solutions in mimetic gravity; rotation curves and wormholes, Classical Quantum Gravity **33**, 125005 (2016).
[35] A. Ganz, P. Karmakar, Sabino Matarrese, and Dmitri Sorokin, Hamiltonian analysis of mimetic scalar gravity revisited, Phys. Rev. D **99**, 064009 (2019).
[36] C. Y. Chen, M. Bouhmadi-López, and P. Chen, Black hole solutions in mimetic Born-Infeld gravity, Eur. Phys. J. C **78**, 59 (2018).
[37] G. G. L. Nashed, Spherically symmetric black hole solution in mimetic gravity and anti-evaporation, Int. J. Geom Met. Mod. Phys **15**, 1850154 (2018).
[38] J. B. Achour, F. Lamy, H. Liu, and K. Noui, Non-singular black holes and the limiting curvature mechanism: A Hamiltonian perspective, J. Cosmol. Astropart. Phys. 05 (2018) 072.
[39] S. Brahma, A. Golovnev, and D.-han Yeom, On singularity-resolution in mimetic gravity, Phys. Lett. B **782**, 280 (2018).
[40] Y. Zheng, L. Shen, Y. Mou, and M. Li, On (in)stabilities of perturbations in mimetic models with higher derivatives, J. Cosmol. Astropart. Phys. 08 (2017) 040.
[41] L. Shen, Y. Zheng, and M. Li, Two-field mimetic gravity revisited and Hamiltonian analysis, J. Cosmol. Astropart. Phys. 12 (2019) 026.
[42] G. G. Nashed, W. E. Hanafy, and K. Bamba, Charged rotating black holes coupled with nonlinear electrodynamics Maxwell field in the mimetic gravity, J. Cosmol. Astropart. Phys. 01 (2019) 058.

[43] A. H. Chamseddine, Viatcheslav Mukhanov, and Tobias B. Russ, Black hole remnants, J. High Energy Phys. 10 (2019) 104.
[44] M. A. Gorji, A. Allahyari, M. Khodadi, and H. Firouzjahi, Mimetic black holes, Phys. Rev. D **101**, 124060 (2020).
[45] A. Sheykhi, Mimetic black strings, J. High Energy Phys. 07 (2020) 031.
[46] A. Sheykhi, Mimetic black holes in $2+1$ dimensions, J. High Energy Phys. 01 (2021) 043.
[47] G. G. L. Nashed and S. Nojiri, Mimetic Euler-Heisenberg theory, charged solutions and multihorizon black holes, Phys. Rev. D **104**, 044043 (2021).
[48] A. H. Chamseddine, Supergravity with mimetic dark matter, Eur. Phys. J. C **81**, 977 (2021).
[49] Y. Zheng, Hamiltonian analysis of mimetic gravity with higher derivatives, J. High Energy Phys. 01 (2021) 085.
[50] H. R. Bakhtiarizadeh, Higher dimensional charged static and rotating solutions in mimetic gravity, Eur. Phys. J. C **82**, 573 (2022).
[51] G. G. L. Nashed, Anisotropic compact stars in the mimetic gravitational theory, Astrophys. J. **919**, 113 (2021).
[52] S. Nojiri and S. D. Odintsov, Mimetic $F(R)$ gravity: Inflation, dark energy and bounce, Mod. Phys. Lett. A **29**, 1450211 (2014).
[53] S. D. Odintsov and V. K. Oikonomou, Accelerating cosmologies and the phase structure of $F(R)$ gravity with Lagrange multiplier constraints: A mimetic approach, Phys. Rev. D **93**, 023517 (2016).
[54] V. K. Oikonomou, Aspects of late-time evolution in mimetic $F(R)$ gravity, Mod. Phys. Lett. A **31**, 1650191 (2016).
[55] V. K. Oikonomou, A note on Schwarzschild de Sitter black holes in mimetic $F(R)$ gravity, Int. J. Mod. Phys. D **25**, 1650078 (2016).
[56] V. K. Oikonomou, Reissner Nordstrom black holes in mimetic $F(R)$ gravity, Universe **2**, 10 (2016).
[57] R. Myrzakulov and L. Sebastiani, Non-local $F(R)$-mimetic gravity, Astrophys. Space Sci. **361**, 188 (2016).
[58] S. D. Odintsov and V. K. Oikonomou, Viable mimetic $F(R)$ gravity compatible with Planck observations, Ann. Phys. (Amsterdam) **363**, 503 (2015).
[59] S. D. Odintsov and V. K. Oikonomou, Unimodular mimetic F(R) inflation, Astrophys. Space Sci. **361**, 236 (2016).
[60] S. D. Odintsov and V. K. Oikonomou, Dark energy oscillations in mimetic $F(R)$ gravity, Phys. Rev. D **94**, 044012 (2016).
[61] S. Nojiri, S. D. Odintsov, and V. K. Oikonomou, Ghost-free $F(R)$ gravity with Lagrange multiplier constraint, Phys. Lett. B **775**, 44 (2017).
[62] S. D. Odintsov and V. K. Oikonomou, The reconstruction of $Rf(\phi)$ and mimetic gravity from viable slow-roll inflation, Nucl. Phys. **B929**, 79 (2018).
[63] S. Bhattacharjee, Inflation in mimetic $f(R,T)$ gravity, New Astron. **90**, 101657 (2022).
[64] A. Z. Kaczmarek and D. Szczesniak, Cosmology in the mimetic higher-curvature $f(R, R_{\mu\nu}R^{\mu\nu})$ gravity, Sci. Rep. **11**, 18363 (2021).
[65] J. Chen, W. Guo, and Y. Liu, Thick branes with inner structure in mimetic $f(R)$ gravity, Eur. Phys. J. C **81**, 709 (2021).
[66] A. V. Astashenok, S. D. Odintsov, and V. K. Oikonomou, Modified Gauss Bonnet gravity with the Lagrange multiplier constraint as mimetic theory, Classical Quantum Gravity **32**, 185007 (2015).
[67] V. K. Oikonomou, Singular bouncing cosmology from Gauss-Bonnet modified gravity, Phys. Rev. D **92**, 124027 (2015).
[68] Y. Zhong and E. Elizalde, De Sitter and power-law solutions in some models of modified gravity, Mod. Phys. Lett. A **31**, 1650221 (2016).
[69] Y. Zhong and D. Saez-Chillon Gomez, Inflation in mimetic $f(G)$ gravity, Symmetry **10**, 170 (2018).
[70] B. C. Paul, S. D. Maharaj, and A. Beesham, Emergent universe scenario in modified Gauss-Bonnet gravity, arXiv:2008.00169.
[71] S. Nojiri, S. D. Odintsov, and V. K. Oikonomou, Mimetic completion of unified inflation-dark energy evolution in modified gravity, Phys. Rev. D **94**, 104050 (2016).
[72] Y. Yang and Y. Gong, The evidence of cosmic acceleration and observational constraints, J. Cosmol. Astropart. Phys. 06 (2020) 059.
[73] U. Seljak, A. Slosar, and P. McDonald, Cosmological parameters from combining the Lyman-alpha forest with CMB, galaxy clustering and SN constraints, J. Cosmol. Astropart. Phys. 10 (2006) 014.
[74] Eugene Oks, Brief review of recent advances in understanding dark matter and dark energy, New Astron. Rev. **93**, 101632 (2021).
[75] P. Peebles, *Principles of Physical Cosmology* (Princeton University Press, Princeton, NJ, 1993).
[76] S. D. M. White and M. J. Rees, Core condensation in heavy halos: A two-stage theory for galaxy formation and clustering, Mon. Not. R. Astron. Soc **183**, 341 (1978).
[77] D. Huterer, David Kirkby *et al.*, Growth of cosmic structure: Probing dark energy beyond expansion, Astropart. Phys. **63**, 23 (2015).
[78] J. Miralda-Escude, The dark age of the universe, Science **300**, 1904 (2003).
[79] R. Abramo, R. Batista, L. Liberato, and R. Rosenfeld, Structure formation in the presence of dark energy perturbations, J. Cosmol. Astropart. Phys. 11 (2007) 012.
[80] S. Planelles, D. Schleicher, and A. Bykov, Large-scale structure formation: From the first non-linear objects to massive galaxy clusters, Space Sci. Rev. **51**, 93 (2016).
[81] T. Naderi, M. Malekjani, and F. Pace, Evolution of spherical overdensities in holographic dark energy models, Mon. Not. R. Astron. Soc. **447**, 1873 (2015).
[82] S. Dutta and I. Maor, Voids of dark energy, Phys. Rev. D **75**, 063507 (2007).
[83] J. Matsumoto, S. Odintsov, and S. Sushkov, Cosmological perturbations in mimetic matter model, Phys. Rev. D **91**, 064062 (2015).
[84] M. Visser, Jerk, snap and the cosmological equation of state, Classical Quantum Gravity **21**, 2603 (2004).
[85] D. Rapetti, S. W. Allen, M. A. Amin, and R. D. Blandford, A kinematical approach to dark energy studies, Mon. Not. R. Astron. Soc. **375**, 1510 (2007).

[86] A. A. Mamon and K. Bamba, Observational constraints on the jerk parameter with the data of the Hubble parameter, Eur. Phys. J. C **78**, 862 (2018).
[87] A. H. Ziaie, H. Moradpour, and H. Shabani, Structure formation in generalized Rastall gravity, Eur. Phys. J. Plus **135**, 916 (2020).
[88] B. Ryden, *Introduction to Cosmology* (Addison-Wesley Press, San Francisco, 2003).
[89] J. H. Wise, Cosmic reionization, Contemp. Phys. **60**, 145 (2019).
[90] N. Kaiser, Clustering in real space and in redshift space, Mon. Not. R. Astron. Soc. **227**, 1 (1987).
[91] S. Tsujikawa, A. Felice, and J. Alcaniz, Testing for dynamical dark energy models with redshift-space distortions, J. Cosmol. Astropart. Phys. 01 (2013) 030.
[92] S. Nesseris, G. Pantazis, and L. Perivolaropoulos, Tension and constraints on modified gravity parametrizations of Geff(z) from growth rate and Planck data, Phys. Rev. D **96**, 023542 (2017).
[93] S. Nesseris and L. Perivolaropoulos, Testing LCDM with the growth function (a): Current constraints, Phys. Rev. D **77**, 023504 (2008).
[94] H. William and P. Schechter, Formation of galaxies and clusters of galaxies by self-similar gravitational condensation, Astrophys. J. **187**, 425 (1974).
[95] L. Liberato and R. Rosenfeld, Dark energy parameterizations and their effect on dark halos, Mon. J. Cosmol. Astropart. Phys. 07 (**2006**) 009.
[96] T. Padmanabhan, *Structure Formation in the Universe* (Cambridge University Press, Cambridge, UK, 1993).
[97] D. Herrera, I. Waga, and S. E. Jorás, Calculation of the critical overdensity in the spherical-collapse approximation, Phys. Rev. D **95**, 064029 (2017).
[98] N. J. Nunes and D. F. Mota, Structure formation in inhomogeneous dark energy models, Mon. Not. R. Astron. Soc. **368**, 751 (2006).
[99] P. T. P. Viana and A. R. Liddle, The cluster abundance in flat and open cosmologies, Mon. Not. R. Astron. Soc. **281**, 323 (1996).
[100] D. N. Spergel, L. Verde, H. V. Peiris *et al.*, First-year Wilkinson microwave anisotropy probe (WMAP) observations: Determination of cosmological parameters, Astrophys. J. Suppl. Ser. **148**, 175 (2003).